Polyhedron 202 (2021) 115218

Contents lists available at ScienceDirect

Polyhedron

journal homepage: www.elsevier.com/locate/poly

Adsorptive capture of perrhenate (ReO_4^-) from simulated wastewater by cationic 2D-MOF BUC-17

Jing Ma [a], Chong-Chen Wang [a,*], Zi-Xuan Zhao [a], Peng Wang [a], Jun-Jiao Li [b], Fu-Xue Wang [a]

[a] Beijing Key Laboratory of Functional Materials for Building Structure and Environment Remediation, School of Environment and Energy Engineering, Beijing University of Civil Engineering and Architecture, Beijing 100044, China
[b] China Aviation Planning and Design Institute (Group) CO., LTD., Beijing 100120, China

ARTICLE INFO

Article history:
Received 18 February 2021
Accepted 10 April 2021
Available online 18 April 2021

Keywords:
BUC-17
Perrhenate
Adsorption
Electrostatic interactions
Ion exchange

ABSTRACT

Water-stable $[Co_3(tib)_2(H_2O)_{12}](SO_4)_3$ (**BUC-17**) was hydrothermally synthesized by adding formic acid as a modulator. The as-prepared **BUC-17**, whose zeta potentials were positive in pH 4.0–10.0, was used as potential adsorbent to capture ReO_4^- ions. The corresponding kinetics behavior and equilibrium isotherm fitted well to the pseudo-second-order and Langmuir model, in which the maximum sorption capacity of **BUC-17** was 401.9 mg ReO_4^- g^{-1} sorbent at 298 K. Additionally, **BUC-17** demonstrated outstanding removal activity in wide range of pH (4.0 – 10.0) and high salinity. The fixed-bed column packed with **BUC-17** powder could continuously eliminate ReO_4^- solution, which provided the possibility to accomplish potentially large-scale application. At last, the adsorption mechanism was proposed, which was the synergism of electrostatic interactions and ion exchange between SO_4^{2-} and ReO_4^-.

1. Introduction

Coal, oil, natural gas and other major energy sources are limited and nonrenewable, and the formed CO_2 from their combustion is deemed to be the main anthropogenic factor of climate change [1,2]. To solve this predicament, nuclear energy, as one of renewable form, has been widely concerned release the pressure of fossil fuels in the short term [3,4]. However, some toxically radioactive wastes generated from the nuclear fuel processing and nuclear accidents pose great threats to both human health and the environment. For example, the radioactive waste ^{99}Tc (Technetium-99) might be produced from fission of ^{235}U (uranium-235) or ^{239}Pu (plutonium-239) [5–7]. ^{99}Tc, with $t_{1/2}$ being 2.13×10^5 y, mainly exists in pertechnetate anion (TcO_4^-), the most stable oxidation state, which poses serious threats to the water environment resulted from its dangerously environmental mobility [8]. Various treatment methods were adopted to remove TcO_4^-/ReO_4^- (as an analog of radioactive TcO_4^-) and the methods that have received much attention are ion exchange [9,10], supramolecular recognition [11], reductive immobilization [12,13] and solvent extraction [14]. The adsorption based on ion exchange is one of the most used methods [15]. The ion exchange materials with high adsorption capacity, fast kinetics rate, and outstanding selectivity attracted increasing attentions. The adsorption rates of anion exchange resins are slow, while the inorganic ion-exchangers displayed unsatisfied adsorption capacity and selectivity especially in high salinity condition [15,16]. Therefore, finding new adsorbents that achieve rapid and efficient remove of TcO_4^- will become necessary.

Metal-organic frameworks, which are porous crystalline materials constructing from metal centers and organic linkers [17–20], have been paid attention by multiple fields like drug delivery [21,22], photocatalysis [23–26], adsorption [27–29], gas separation [30,31] and so on [32,33], due to their merits of the inherent porous structures, thermal stability, extremely large surface areas and adjustable pore size [17,34]. Considering the anionic properties of TcO_4^-/ReO_4^-, tremendous efforts were committed to the evolution of cationic framework materials due to their strong electrostatic attractions or host guest interactions [35]. As a subclass of MOFs, cationic MOFs are attracting increasing interest, which are composed of positively charged main frameworks stabilized by the short-interactions of charge counter anions in pores or interlayer spaces [14,36]. At present, some cationic MOF materials for removing TcO_4^-/ReO_4^- have been reported. Banerjee et al.[37] reported the ReO_4^- exchange properties of a cationic zirconium-based MOF, UiO-66-NH^{3+}, which has an uptake capacity of 159 mg g^{-1} with slow adsorption rate for more than 24 h. Li et al.[38] prepared the first mesoporous cationic MOF, SCU-8, and evaluated the uptake capabilities for ReO_4^-. Although it has a fast adsorption rate, its adsorption performance in high salinity wastewater has not been explored. Zhu et al. [39], Sheng et al. [40] and Shen et al. [41] reported several water-stable cationic MOFs, SCU-101, SCU-102

* Corresponding author.
E-mail address: wangchongchen@bucea.edu.cn (C.-C. Wang).

https://doi.org/10.1016/j.poly.2021.115218
0277-5387/

and SCU-103, the maximum sorption capacities are 247 mg g^{-1}, 291 mg g^{-1} and 318 ± 8 mg g^{-1}, respectively. Mei et al. [14] reported a CB8-based cationic supramolecular metal–organic framework, SCP-IHEP-1, which has an uptake capacity of 211 mg g^{-1}. It is necessary to search for cationic MOF materials with higher adsorption capacity and efficient removal of TcO_4^-/ReO_4^- in high salinity wastewater.

The highly water stable **BUC-17** was synthesized under hydrothermal conditions [28]. At first, we found 1,3-adamantanedicarboxylic acid can be used as catalyst and regulator to produce **BUC-17** [28]. Then, our group modified the synthesis method to prepare **BUC-17** powder without 1,3-adamantanedicarboxylic acid as catalyst and regulator [42]. However, we didn't harvest pure **BUC-17** without any impurities via the above-stated synthetic methods, which motivated us to further optimize the synthesis strategy. Within this paper, pure **BUC-17** crystals free of any impurities were synthesized by adding formic acid to modulate its morphology. **BUC-17** was previously used as adsorbents to adsorb anionic Congo red (CR) [28], $Cr_2O_7^{2-}$ [43], and AsO_4^{3-} [42], due to the charge-balancing SO_4^{2-} anions contained in the pores of **BUC-17** can be exchanged out. From this point, **BUC-17** might be effective to capture the radioactive TcO_4^-. However, the experiments concerning TcO_4^- can't be conducted in most ordinary laboratories. Performing technetium experiments in ordinary laboratories will cause environmental pollution problems, due to its strong radioactivity, it will have a certain impact on the health of the experimenters. Generally, ReO_4^- is widely selected as TcO_4^- analog due to their similar chemical properties and ionic radius [44]. Within this paper, the as-prepared **BUC-17** was used to capture ReO_4^- in both batch and continuous experiments, in which the adsorption kinetics, thermodynamics and the effects of pH and coexisting ions on the adsorption behavior were studied. Finally, the possible adsorption mechanism was put forward and verified.

2. Experimental

The chemicals and the characterization instruments were listed in Supplementary Information (SI).

2.1. BUC-17 synthesis

The **BUC-17** was produced following the previous reported procedure with some modifications [28]. Briefly, 1,3,5-tris(1-imidazolyl) benzene (tib: 0.3 mmol, 0.0829 g) and $CoSO_4{\cdot}7H_2O$ (0.3 mmol, 0.0843 g) were dissolved in 10.0 mL deionized H_2O, and formic acid (0.3 mmol, 13 μL) was put into the mixture instead of 1,3-adamantanedicarboxylic acid to modulate the morphology. The above solution was transferred into the 25 mL Teflon-lined stainless steel Parr bomb, which was heated at 140 °C for 72 h, and then cooled down to room temperature naturally for about 2 h. Finally, the pure **BUC-17** crystals (yield 61% based on $CoSO_4{\cdot}7H_2O$) with regular hexagonal prism shape were obtained via filtration. FTIR (KBr) cm^{-1}: 3381, 3131, 1672, 1623, 1546, 1515, 1358, 1317, 1273, 1258, 1182, 1125, 1078, 1012, 974, 934, 849, 817, 758, 664, 611, 448.

The stability of **BUC-17** was tested by soaking it in H_2SO_4 or NaOH solution with pH values from 4.0 to 10.0 under continuous stirring for 12 h. Finally, PXRD test was conducted to check the stability of treated **BUC-17**.

2.2. Adsorption experiments

ReO_4^- (Re(VII)) was adopted as anionic pollutant model to evaluate the adsorption activity of **BUC-17**. Kinetic studies were carried out by adding 50 mg **BUC-17** into 200.0 mL of 10 mg L^{-1} to 100 mg L^{-1} ReO_4^- solution (calculated by Re(VII)) at pH = 5.0, which was stirred for 15 h in constant temperature water bath shaker at 25 ℃, and the rotation speed was 170 r min^{-1}. The sorption isotherm experiments of **BUC-17** on ReO_4^- were carried out by varying initial ReO_4^- concentrations (10–150 mg L^{-1}) at pH = 5. In a typical run, exact amounts of **BUC-17** (50 mg) and 200.0 mL ReO_4^- solution were stirred for equilibrium times. During the adsorption process, 4.0 mL sample was separated with 0.22 μm springe filter from the treated solution at regular intervals. The residual concentrations of Re(VII) in aqueous solution were monitored by inductively coupled plasma-optical emission spectroscopy (ICP-OES, ICP-5000, Focused Photonics Inc., China). The adsorption capacity was calculated by Eq. S1.

2.3. Fixed bed column investigation

In order to study the potentially practical application of **BUC-17**, the fixed-bed column experiments were carried out in solid phase extraction (SPE) column. 2.0 g **BUC-17** powder (with the particle size from 0.2 to 2 μm) was packed into the commercially available empty column. The solution containing 50 mg L^{-1} ReO_4^- was pumped through the SPE column at a flow rate of 0.4 mL min^{-1} via automatic vacuum. Turn on the vacuum pump and control the pressure by adjusting the purge valve to ensure a constant flow rate which was determined by calculating the flow rate of the solution for a certain period of time. During the adsorption process, 4.0 mL sample was collected at regular intervals. The residual Re (VII) concentrations in the samples were monitored by ICP-OES.

3. Results and discussion

3.1. Characterization

The powder X-ray diffraction (PXRD) patterns of as-obtained **BUC-17** completely corresponded with the simulated ones from the single-crystal structure data (CCDC 1482297) as illustrated in Fig. 1a, indicating the high purity of the as-obtained **BUC-17**. The PXRD results of **BUC-17** after being soaked in acid/alkaline solution (pH = 4.0–10.0) for 12 h matched perfectly with that of fresh **BUC-17** (Fig. 1a), demonstrating it remained intact in both acidic and alkaline environment. And the XRD pattern for the as-synthesized and simulated **BUC-17** reveal characteristic peak at 7.5° corresponding to diffraction planes of (210). The peak at 9.0° in the PXRD patterns of the treated **BUC-17** had a slight displacement to higher angles compared to that of synthesized and simulated samples (peak at 7.5°). Such a right-shift of the diffraction peak is expected as there is a high concentration of OH^- in deionized water, and OH^- with a small ionic radius replaces part of the SO_4^{2-} with a large ionic radius in **BUC-17** [45]. Both the fluorescence microscopy images and SEM images directly showed that **BUC-17** crystals exhibit the regular hexagonal prism (Fig. 1b and 1c). It can be found that the **BUC-17** powder after grinding treatment demonstrated irregular morphology under SEM observation (Fig. 1d).

3.2. Adsorption performance

3.2.1. Adsorption kinetics

To quickly test the adsorption performance of **BUC-17**, the Congo red (CR) was selected as pollutant model. It was found that>99.4% CR can be adsorbed by as-prepared **BUC-17** within 1 min (Fig. S1), which was faster than that of **BUC-17** (3 min) synthesized without adding formic acid [28]. Subsequently, **BUC-17** was adopted to remove ReO_4^- in simulated wastewater (different concentrations of ReO_4^- solution). To understand the adsorption

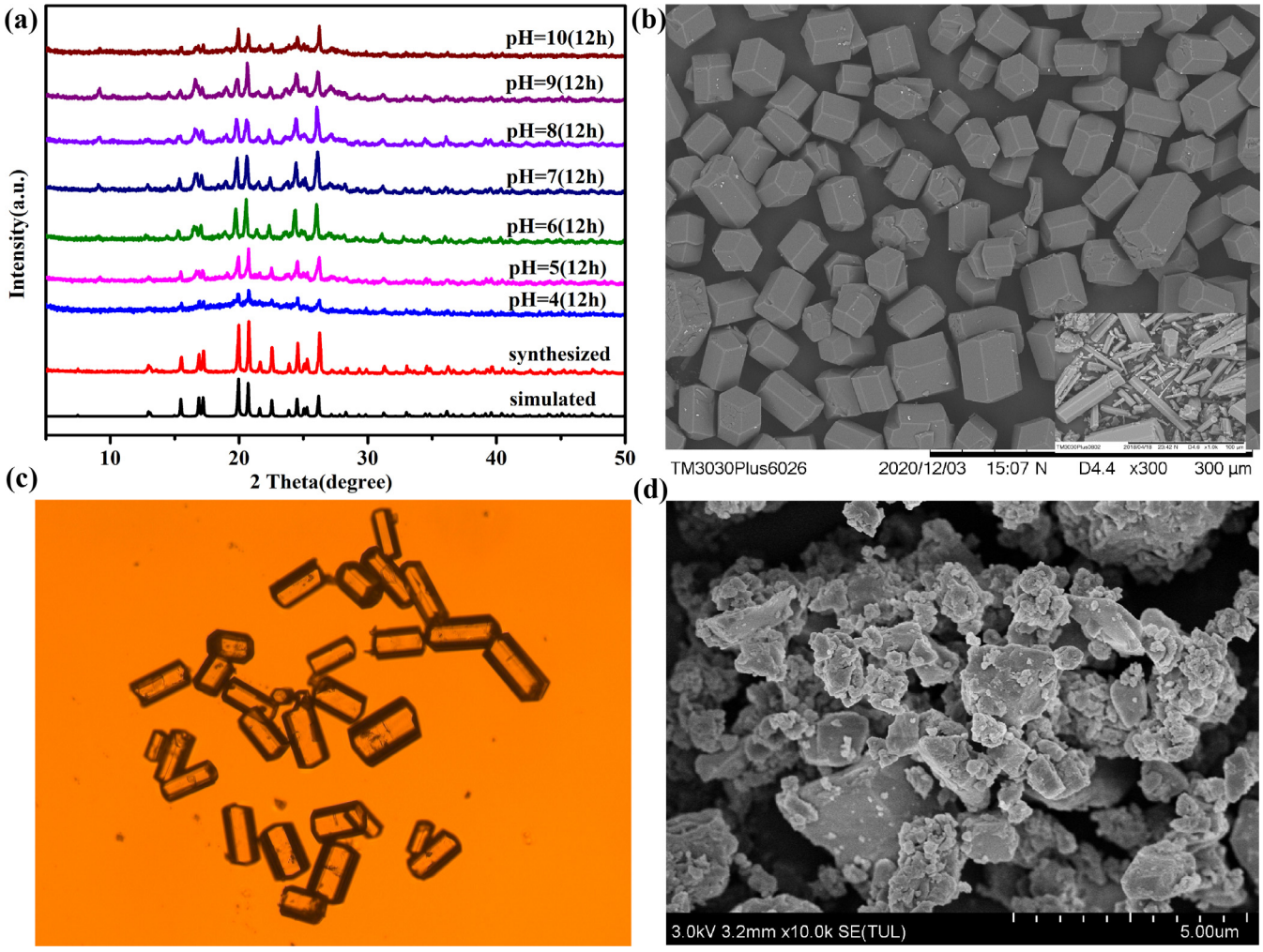

Fig. 1. (a) The PXRD patterns of **BUC-17** before and after being treated by acidic or alkaline solution, and the simulated one from single crystal date; (b) SEM image of **BUC-17** crystals synthesized in this work and (inset) previous method [43]; (c) fluorescence microscopy image of **BUC-17** crystals; (d) SEM image of **BUC-17** powder obtained from grinding treatment.

process and mechanism, the adsorption kinetics like the pseudo-first-order, pseudo-second-order as well as intraparticle diffusion models (as listed in Eqs. S2-S4) were calculated [46]. The rate limiting step is deemed to be diffusion and mass transfer of the adsorbate to the adsorption site in first-order model, and chemical adsorption in the second-order model [47]. From Fig. 2b, 2c and Table 2, batch kinetics experiment results demonstrated that the adsorption of ReO_4^- onto **BUC-17** obeyed the pseudo-second-order model. The obtained R^2 values are above 0.999 at the initial ReO_4^- concentrations of 10 mg L^{-1} to 100 mg L^{-1}, demonstrating that the adsorption process was chemical adsorption [48,49].

Additionally, the Weber–Morris model [50] was used to understand the intra-particle diffusion in the adsorption process. If the rate controlling step is intra-particle diffusion, the plot of the change of (q_t) (mg g^{-1}) with $t^{1/2}$ (the square root of contact time) will display a straight line through the origin [51]. As depicted in Fig. 2d, the adsorption behaviors of **BUC-17** toward ReO_4^- could be mainly divided into two sub-processes: the linear portion ended with smooth curve and a linear part. The initial curved part of the plot represents the boundary layer effect, while the second linear portion can be ascribed to diffusion within the intraparticle or the pore [52]. The linear portion of plot is not through the origin, implying that the intraparticle diffusion is not the only rate limiting step [53]. The results showed that both surface adsorption and intra-particle diffusion are the main factors determining the reaction rate [43].

The adsorption rate is a key factor to determine whether or not an adsorbent can be utilized to efficiently dislodge pollutants [54]. Fig. 2a revealed that the adsorption capacity of ReO_4^- on **BUC-17** increased with the increase of contact time. Up to 98% ReO_4^- with initial concentration of 10 mg L^{-1} can be removed by **BUC-17** within 6 min. For the aqueous solution with initial ReO_4^- concentrations of 100 mg L^{-1}, 92% removal efficiency can be achieved within 100 min, and complete equilibrium can be basically achieved in 280 min (>97%), as the reaction time continues until 8 h, the concentration of the remaining ReO_4^- in the solution is only reduced by about 2 mg L^{-1}. The kinetics rate of ReO_4^- exchange over **BUC-17** is superior to those of other cationic adsorbents including but not limited to SLUG-21, NDTB-1, UiO-66-NH_3^+ and TJNU-216 (Table 1). Although **BUC-17** had a slower adsorption rate compared to some materials, its adsorption capacity was higher.

3.2.2. Adsorption isotherms

To acquire q_{max} (the maximum sorption capacity) of **BUC-17**, the adsorption isotherm investigations were conducted [54]. Three isotherm models like Langmuir, Freundlich, along with Dubinin–Radushevich isotherm equations (expressed as Eqs. S5–S9) were used to describe the adsorption isotherms behaviors in detail.

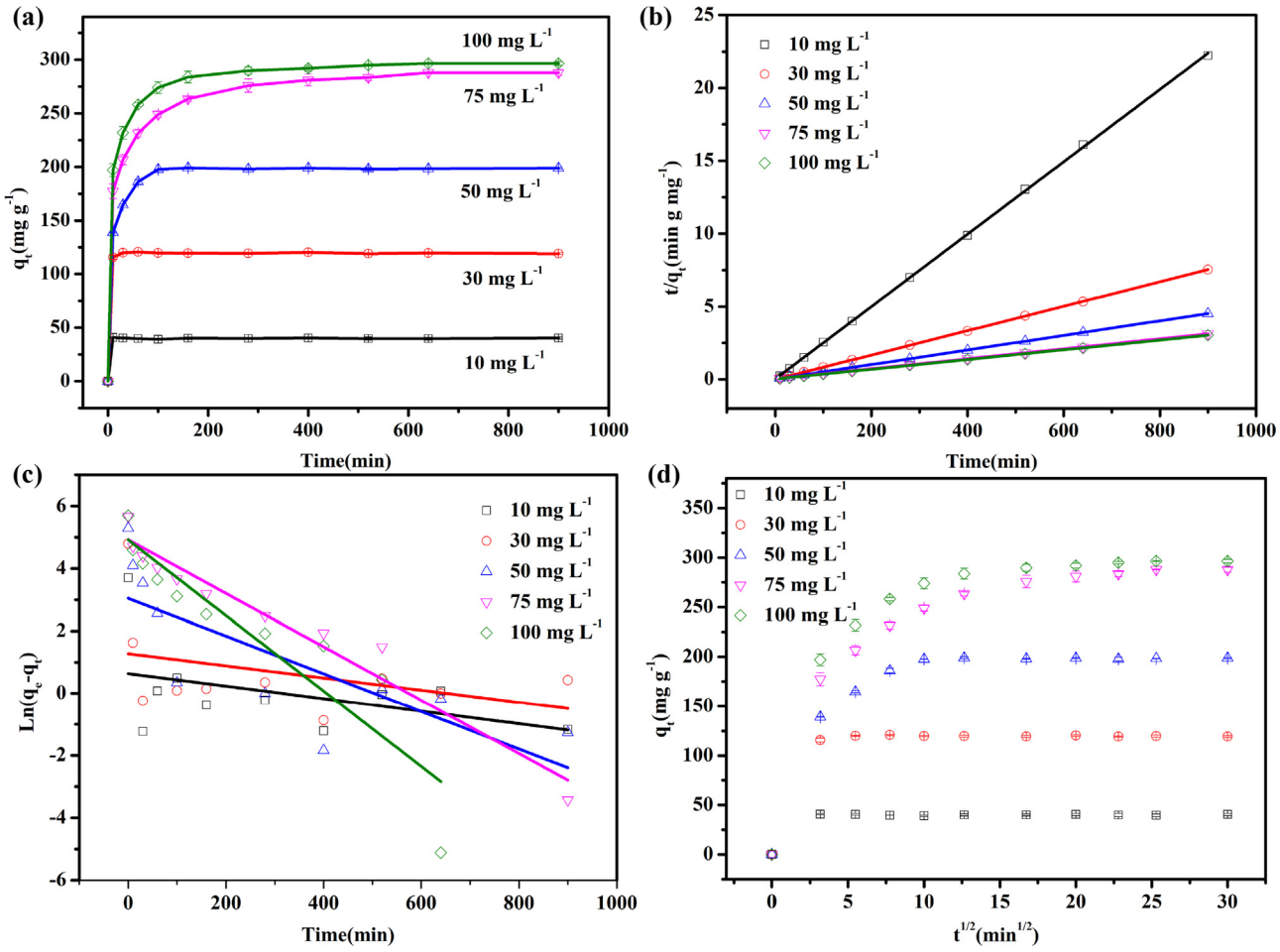

Fig. 2. (a) The adsorption capacities of **BUC-17** toward ReO_4^- with different initial concentrations (pH = 5.0, T = 298 K); the matching results for (b) Pseudo-first-order model and (c) pseudo-second-order model of **BUC-17** toward ReO_4^- (298 K); (d) Intra-particle diffusion plot for **BUC-17** uptake of ReO_4^- (298 K).

Table 1
The adsorption capacities and kinetics rates toward ReO_4^- over some counterpart adsorbents.

Adsorbents	Adsorption capacity (mg g^{-1})	Equilibrium time	Refs.
LDH	130	NA	[55]
SLUG-21	602	48 h	[56]
SCP-IHEP-1	211	> 10 min	[14]
NDTB-1	49.4	> 36 h	[57,58]
NU-1000	210	5 min	[15]
IIP-3	84.38	15 min	[59]
DNOA-OCS	222.69	NA	[60]
NZVI/rGOs	115.25	50 min	[61]
SCU-101	247	10 min	[39]
UiO-66-NH_3^+	159	> 24 h	[37]
TJNU-216	417	6 h	[62]
BUC-17	401.9	280 min	This work

The adsorption isotherms behaviors of **BUC-17** at different temperatures like 288 K, 293 K, 298 K, 303 K and 308 K with varying initial concentrations were depicted in Fig. 3.

As presented in Table 3, the higher R^2 values implied that the Langmuir model matched more perfect than other isotherm models [63], which was further affirmed by perfect match between the maximum adsorption capacities calculated and the experimental ones. The q_{max} values acquired by the Langmuir model decreased with the temperature, demonstrating that the low temperature might favor the exothermic adsorption. As revealed by the sorption isotherm experiment, the q_{max} of **BUC-17** is 401.9 mg ReO_4^- g^{-1} sorbent equivalent of 299.1 mg Re g^{-1} sorbent. Significantly, the q_{max} value of **BUC-17** was appreciably higher than those of most counterpart adsorbents reported previously like SLUG-21 and NU-1000 (Table 1). The Langmuir model supposes that the sorption process

Table 2
Kinetic parameters related to adsorption with varying concentrations of ReO_4^- onto **BUC-17** at 298 K.

C_0 (mg L^{-1})	Pseudo-first-order			Pseudo-second-order			measured value (mg g^{-1})
	K_1 (min^{-1})	q_e (mg g^{-1})	R^2	K_2 (min^{-1})	q_e (mg g^{-1})	R^2	
10	0.00202	1.8926	0.07629	0.01981	40.2576	0.99981	40.7992
30	0.00203	2.9869	0.05786	0.02208	119.9041	0.99998	120.3658
50	0.00605	21.0462	0.55756	0.00157	199.6008	0.99995	199.1568
75	0.00857	137.351	0.94721	0.00024	292.3977	0.99983	289.6496
100	0.01211	136.594	0.83001	0.00039	299.4012	0.99997	299.1152

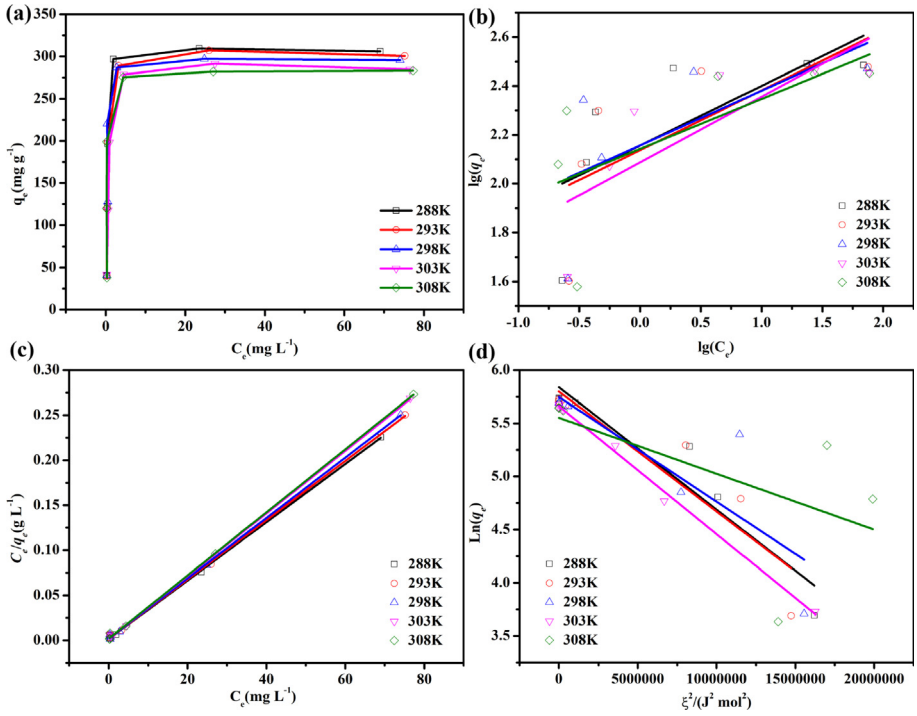

Fig. 3. (a) The Equilibrium data of the adsorption process at varying temperatures; (b) Langmuir, (c) Freundlich, and (d) Dubinin–Radushevich (D–R) isotherms for adsorption ReO_4^- by **BUC-17**.

Table 3
Constants of isotherm models for ReO_4^- adsorption by **BUC-17** at various temperatures.

T/K	Langmuir			Freundlich			D–R		
	K_L (L mg^{-1})	q_m (mg g^{-1})	R^2	K_f (L g^{-1})	1/n	R^2	K_{DR}	E (KJ mol^{-1})	R^2
288	1.946	309.6	0.9995	143.361	0.244	0.4110	1.151×10^{-7}	2.085	0.8927
293	1.891	304.0	0.9993	137.227	0.245	0.4349	1.129×10^{-7}	2.105	0.8158
298	1.811	298.5	0.9995	143.499	0.224	0.3362	9.834×10^{-8}	2.255	0.6394
303	1.735	288.2	0.9995	122.231	0.269	0.5509	1.202×10^{-7}	2.040	0.9949
308	1.659	285.7	0.9993	138.851	0.205	0.3097	5.260×10^{-8}	3.083	0.2388

occurs on surface of adsorbents via monolayer sorption [39]. The sorption isotherm of **BUC-17** is suitable with Langmuir model, indicating that uniform monolayer sorption mode is suitable to interpret the sorption behavior of **BUC-17** [14].

3.2.3. Thermodynamic parameters

According to Langmuir adsorption isotherm, all the thermodynamic parameters like ΔG^o (the standard free energy), ΔH^o (enthalpy) and ΔS^o (entropy) were calculated via Eqs. S10 and S11 and listed in Table 4. Significantly, the value of free energy (ΔG^o) between −20 and 0 kJ mol^{-1} indicates that the physical adsorption plays a leading role. While for chemisorption, the corresponding ΔG^o value ranges from −80 to −400 kJ mol^{-1} [64,65]. In this study, the negative value of ΔG^o from −30.65 kJ mol^{-1} to −32.37 kJ mol^{-1} demonstrated that the sorption process was spontaneous as the result of physical adsorption and chemical adsorption [27,66]. The ΔH^o (-5.97 kJ mol^{-1}) of the adsorption between **BUC-17** and ReO_4^- was negative, indicating the exothermic nature of sorption process [67]. The positive ΔS^o (85.76 J mol^{-1} K^{-1}) implied that the randomness increment occurred during the adsorption process [66,68]. These results demonstrated that the sorption of **BUC-17** toward ReO_4^- was spontaneous, exothermic as well as the random increment process.

3.3. Influencing factors

3.3.1. Influences of BUC-17 dosage and initial ReO_4^- concentration

The dosage of **BUC-17** and the initial concentration of ReO_4^- have an important influence on the ReO_4^- removal efficiency. Fig. 4a and 4b showed the impact of the **BUC-17** adsorbent dosage (from 200.0 to 300.0 mg L^{-1}) and initial ReO_4^- (from 10 to 50 mg L^{-1}) on the sorption capacity and elimination efficiency. For the same initial ReO_4^- concentration like 10 mg L^{-1}, the adsorption capacity decreased from 46.2 mg g^{-1} to 33.4 mg g^{-1} when **BUC-17** dosage increased from 200.0 to 300.0 mg L^{-1}, due to that the added adsorbent exceeded the required dosage corresponding to the specific ReO_4^- amount [43]. For different initial concentration and adsorbent dosage, **BUC-17** can achieve good ReO_4^- good removal efficiency as illustrated in Fig. 4b.

3.3.2. Effect of pH on ReO_4^- sorption in BUC-17

pH might exert noticeable influence to both the ζ (zeta) potential of the adsorbent and the existence form of the target pollutants [54,69]. The ReO_4^- solution with C_0 = 50 mg L^{-1} and initial pH of 5.3 ± 0.3 was used to test the pH influence to the adsorption performance by adjusting the pH of the solution with H_2SO_4 and NaOH aqueous solution, respectively. The results revealed that **BUC-17**

Table 4
Thermodynamic parameters of the adsorption behavior over **BUC-17** toward ReO_4^-.

T/K	K_L (L mol^{-1})	ΔG^o (kJ mol^{-1})	ΔS^o (J mol^{-1} K^{-1})	ΔH^o (kJ mol^{-1})
288	362318.44	−30.65	85.76	−5.97
293	352081.05	−31.11		
298	337185.65	−31.54		
303	323069.15	−31.96		
308	308874.17	−32.37		

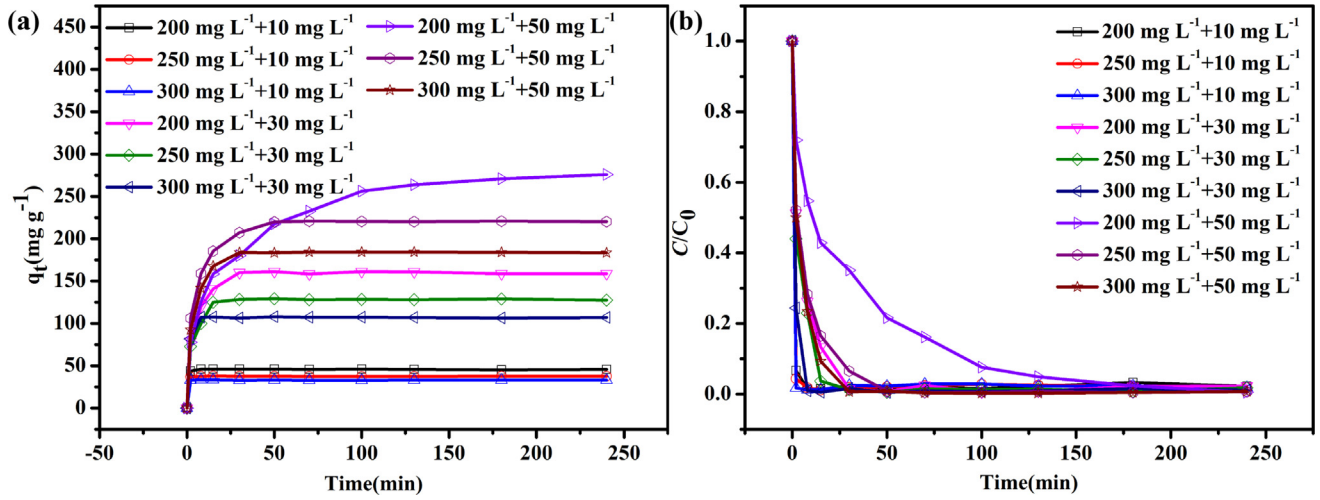

Fig. 4. (a) The sorption capacities and (b) elimination efficiencies of **BUC-17** at different adsorbent dosages (200–300 mg L^{-1}) and initial ReO_4 concentrations (10–50 mg L^{-1}).

demonstrated outstanding removal efficiency toward ReO_4^- in a wide range of pH from 4.0 to 10.0. The presence of $-NH_2$ in **BUC-17**, which was derived from the ligand tib used in the synthesis process, made **BUC-17** dissolve under acidic conditions (pH $\leq$ 3). At the same time, 40 mg **BUC-17** was added to 50 mL of alkaline aqueous solution with pH = 11 and stirred for 12 h. By comparing the processed **BUC-17** with the simulated XRD in Fig. S2, it was found that **BUC-17** cannot exist stably under alkaline conditions (pH $\geq$ 11). As depicted in Fig. 5a, the removal efficiencies toward ReO_4^- over **BUC-17** were maintained at the level of > 98.7% in the pH range of 4.0 to 10.0, indicating that pH value exerted negligible effect on the adsorption process. It can be ascribed to that **BUC-17** adsorbent is positively charged (positive ζ potential) in the pH range of 4.0 to 10.0 [28,43].

3.3.3. Effect of co-existing ions

Generally, there are a large amount of excessive competitive anions like NO_3^-, SO_4^{2-} and Cl^- [35] in the streams containing the radioactive nuclear waste. In order to investigate the effect of co-existing ions, **BUC-17** with dosage of 50.0 mg was increased to 200.0 mL solution containing 0.055 mmol L^{-1} ReO_4^- with and without co-existent anions, in which the molar ratios of different coexistent anions to ReO_4^- controlled to 10:1. As shown in Fig. 5b, NO_3^-, SO_4^{2-} and Cl^- exhibited insignificant impact on the adsorption activity of **BUC-17** as adsorbent, in which the ReO_4^- uptake efficiency over **BUC-17** can reach >98% in the presence of different ions. For certain types of nuclear waste streams like Hanford waste, the excessive NO_3^- and SO_4^{2-} light affect the removal performance of TcO_4^- over adsorbents [35]. Therefore, the effect on the adsorption activity of **BUC-17** toward ReO_4^- resulted from NO_3^- and SO_4^{2-} with high concentration was investigated. As depicted in both Fig. 5c and 5d, the removal efficiencies remain >97% for the molar ratios of NO_3^-/ReO_4^- ranging from 1:1 to 100:1, and >96% for the molar ratios of SO_4^{2-}/ReO_4^- in the range of 1:1 to 6000:1. When the molar ratio of NO_3^-/ReO_4^- was adjusted to 100:1, the removal efficiency of **BUC-17** (97.1%) was higher than those of SCU-102 (93.8%) [40] and SCU-103(>88%) [35]. Impressively, when SO_4^{2-} is present in 6000 fold times of ReO_4^-, **BUC-17** can still remove 96.5% ReO_4^- from the simulated wastewater, which was better than both SCU-101(80%) [39] and SCU-103(82%) [35]. These excited results indicate that **BUC-17** can accomplish high selectivity toward ReO_4^-, which can accomplish effective ReO_4^- elimination from high salinity wastewater.

3.4. Fixed-bed column experiments

In order to develop friendly method for practical operation, the continuous fixed-bed column experiment was carried out, in which the **BUC-17** adsorbent can continuously contact with ReO_4^- ions in aqueous solution. The adsorption behavior and efficiency could be described by the emerge time of breakthrough and the shape of breakthrough plot, which can be used to determine the service time of fixed-bed [27]. The breakthrough experiment of 50 mg L^{-1} ReO_4^- solution flowing over the fixed bed packed with **BUC-17** particles with a flow rate of 0.4 mL min^{-1} at ambient temperature shows that the removal efficiency is up to 97.6% with residual ReO_4^- concentration being 1.11 mg L^{-1} (Fig. 6a, 6b and Video 1). The breakthrough curve displaying the relationship between concentration ratios (C/C_0) of the effluent and the reaction time (T) increased sharply after 75.5 h, indicating quick mass transfer and adsorption kinetics [70,71]. With the increase of adsorbent (**BUC-17**) loading, the adsorption capacity and adsorption time may further increase [27]. The thrilling results demonstrated that **BUC-17** is a potential adsorbent to remove ReO_4^- with high concentration.

3.5. Proposed adsorption mechanism

The BET surface area of **BUC-17** is 1.76 m^{2}g^{-1}, demonstrating that its outstanding adsorption performance toward ReO_4^- could not be ascribed to its porosity [28]. Meanwhile, the hexagonal pore size of **BUC-17** was *ca.* 10.38 nm, which belonged to the range of mesoporous (Fig. S3). The mesoporous effect is also beneficial to

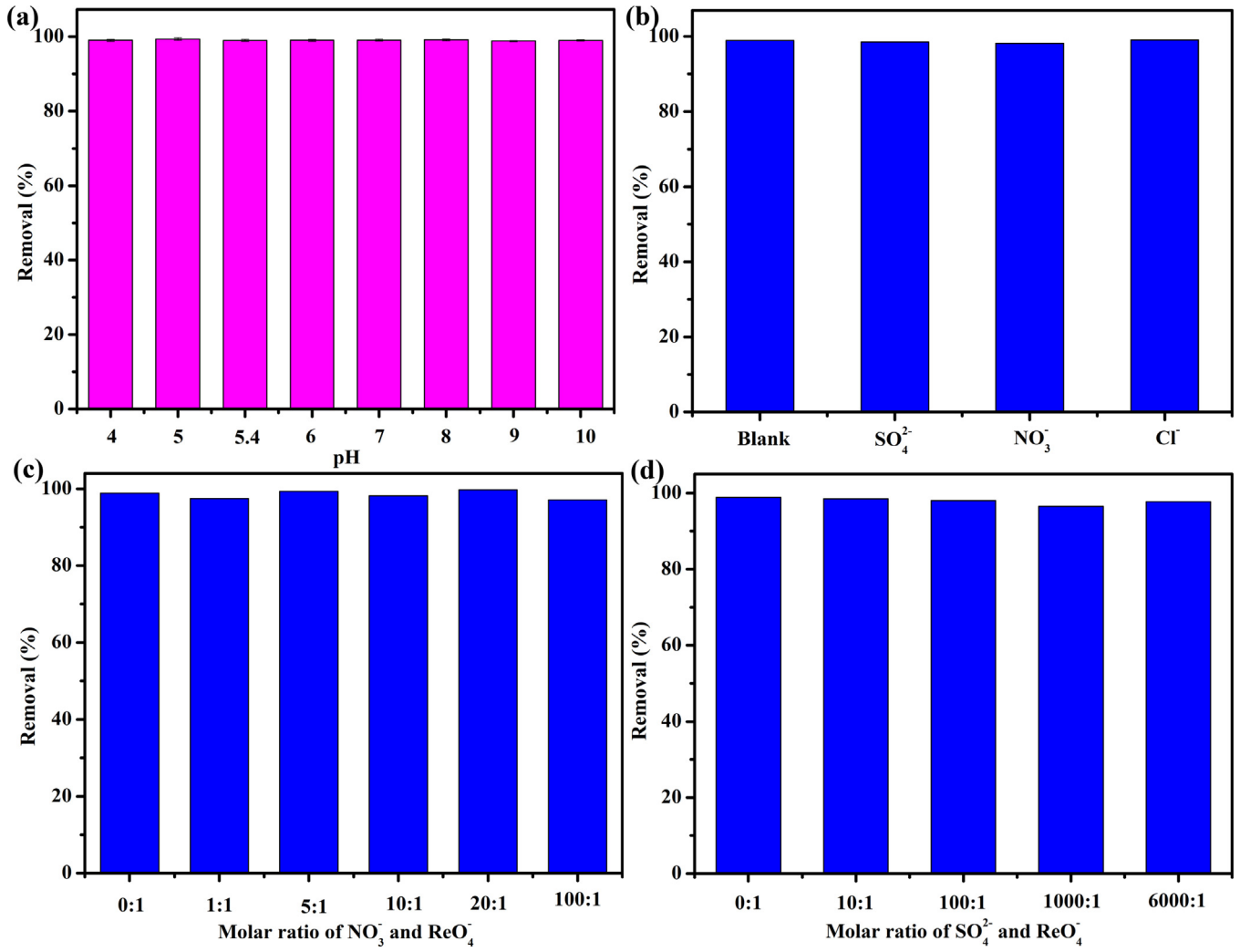

Fig. 5. (a) The influence of pH on the adsorption capacity of ReO_4^- (C_0 = 50 mg L^{-1}); (b) influences of various competing anions on the uptake of ReO_4^- by **BUC-17**; effect of excessive (c) NO_3^- and (d) SO_4^{2-} on the ReO_4^- exchange.

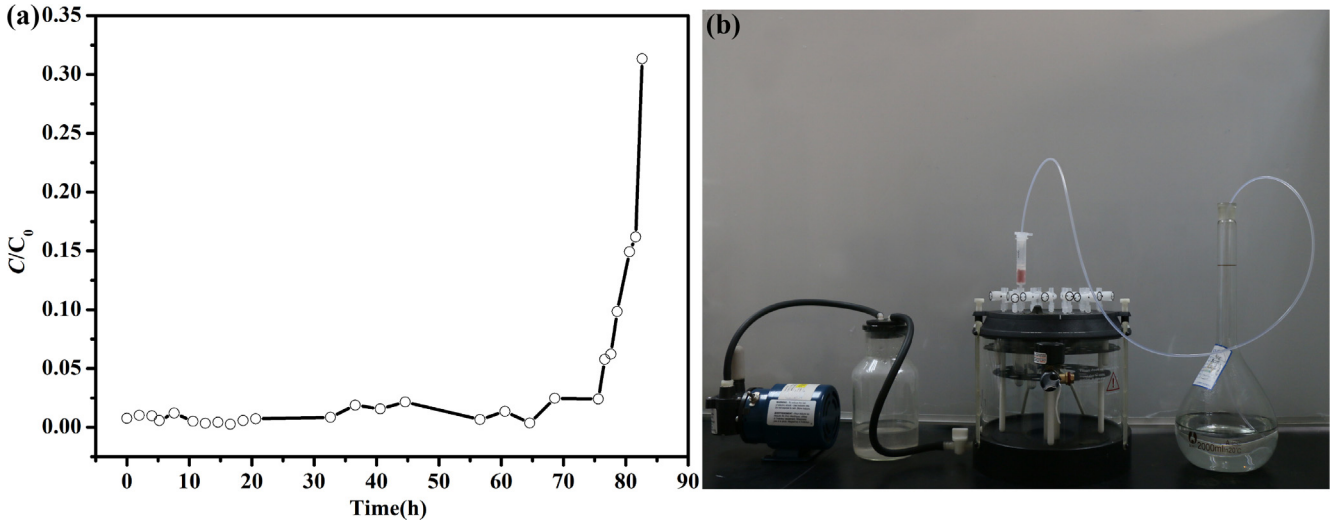

Fig. 6. (a) Breakthrough curves of ReO_4^- over **BUC-17**; (b) equipment of fixed-bed column study.

improve the adsorption activity [72]. The zeta potentials demonstrated that the high removal efficiency of ReO_4^- might be assigned to electrostatic interaction [28,43]. Besides, the uncoordinated SO_4^{2-} counter-anions in the **BUC-17** structure could be exchanged out with the ReO_4^- anions during adsorption process. The decrease in the adsorption efficiency from 98.9% in deionized water to 91.2%

in saturated K_2SO_4 aqueous solution within 50 min supported the interpretation (Fig. 9d).

To further expound the adsorption mechanism of ReO_4^- onto **BUC-17**, some characterizations like PXRD, FTIR, SEM-EDS and XPS of **BUC-17** were carried out. The PXRD of **BUC-17** were fundamentally identical before and after adsorption of ReO_4^- directly showing that **BUC-17** exhibited great stability during the adsorption process (Fig. 7a). As illustrated in Fig. 7b and 7c, the uptake of ReO_4^- onto **BUC-17** was confirmed by the presence of characteristic FRIT peak (907 cm^{-1}) of ReO_4^- and the presence of Re in SEM-EDS mapping after adsorption [14,15,35]. The peak at 3131 cm^{-1} is assigned as the aromatic C—H stretch modes [73]. And the peak at 664 cm^{-1} correspond to the stretching vibrations of Co(II)–O [74]. From Fig. 8, the content of S element after the adsorption decreased while the Re element increased could be observed from EDS also revealed the existence of ion-exchange. The presence of Re element in XPS spectrum (Fig. 9a) also confirmed the sorption of ReO_4^-, and the uncoordinated SO_4^{2-} being exchanged out from **BUC-17** was evidenced by the decreased S 2p peak intensity. As shown in Fig. 9b, the peak located at 44.8 eV is ascribed to Re

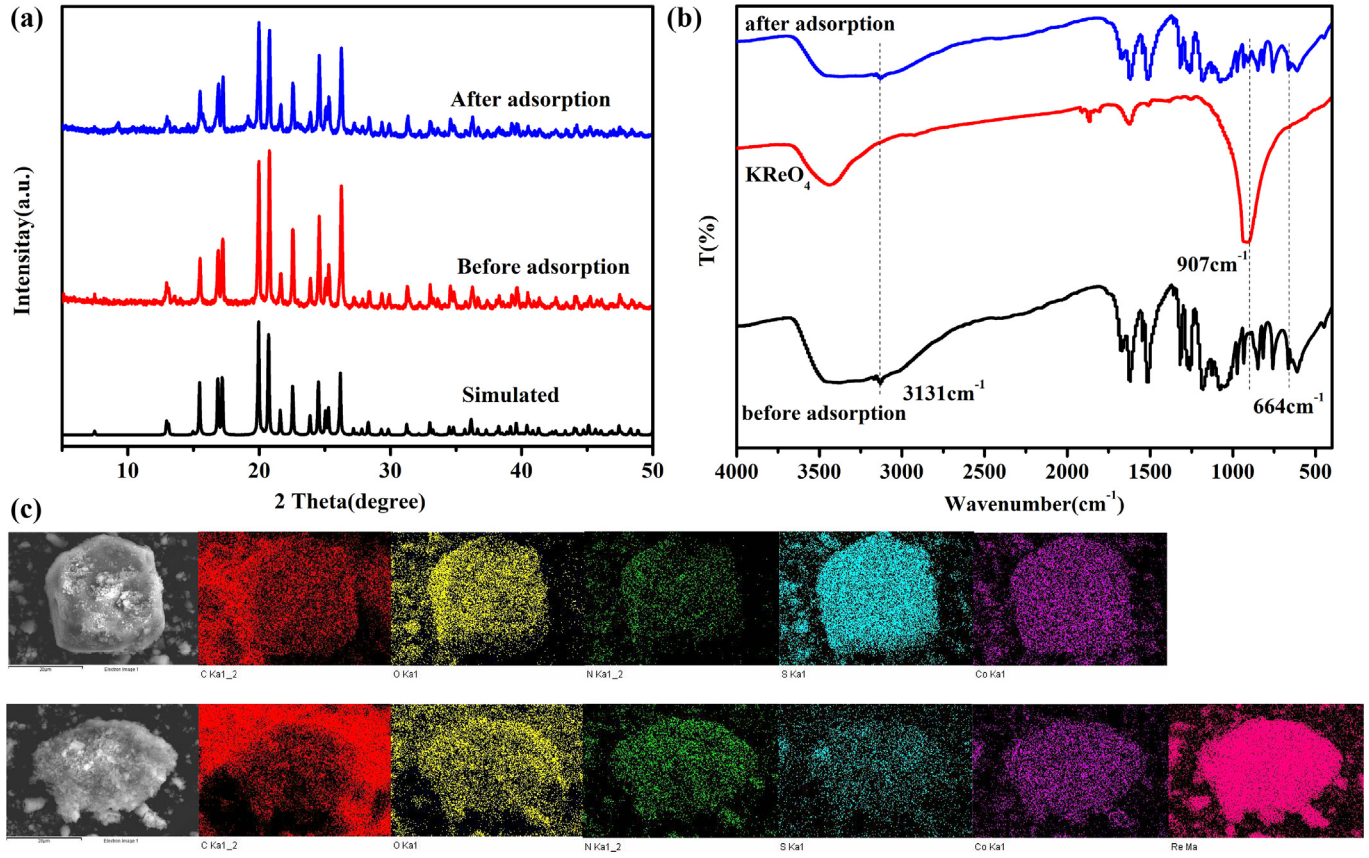

Fig. 7. (a) The PXRD patterns of **BUC-17** of simulated, as-synthesized and after adsorption; (b) the FTIR spectra of potassium perrhenate, along with **BUC-17** before and after adsorption; (c) SEM- Elemental mapping of C, N, O, S, Co and Re.

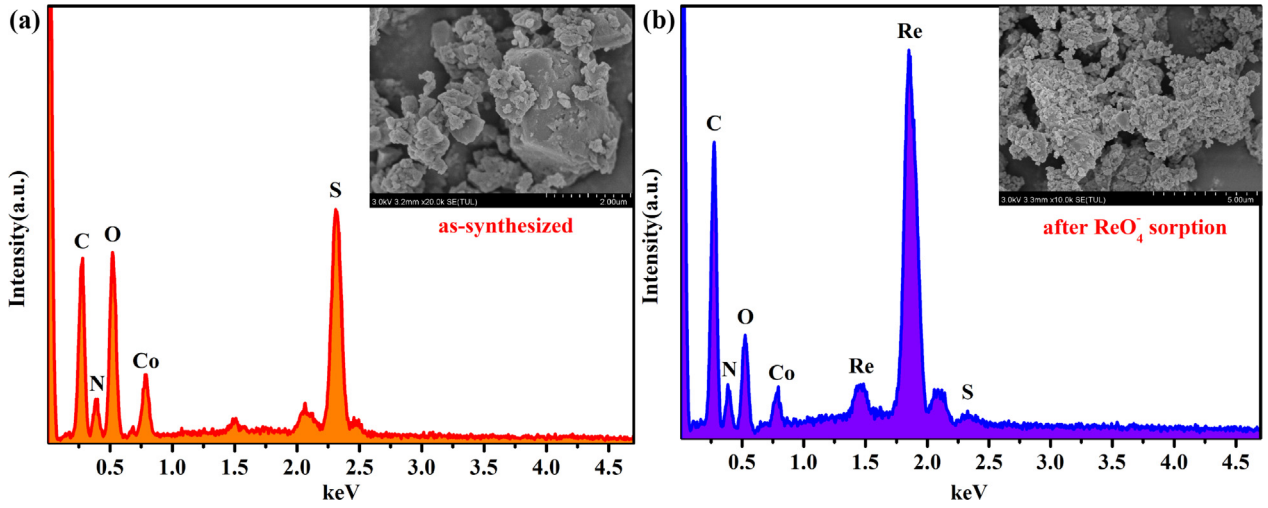

Fig. 8. EDS of **BUC-17** before (a) and after (b) ReO_4^- exchange.

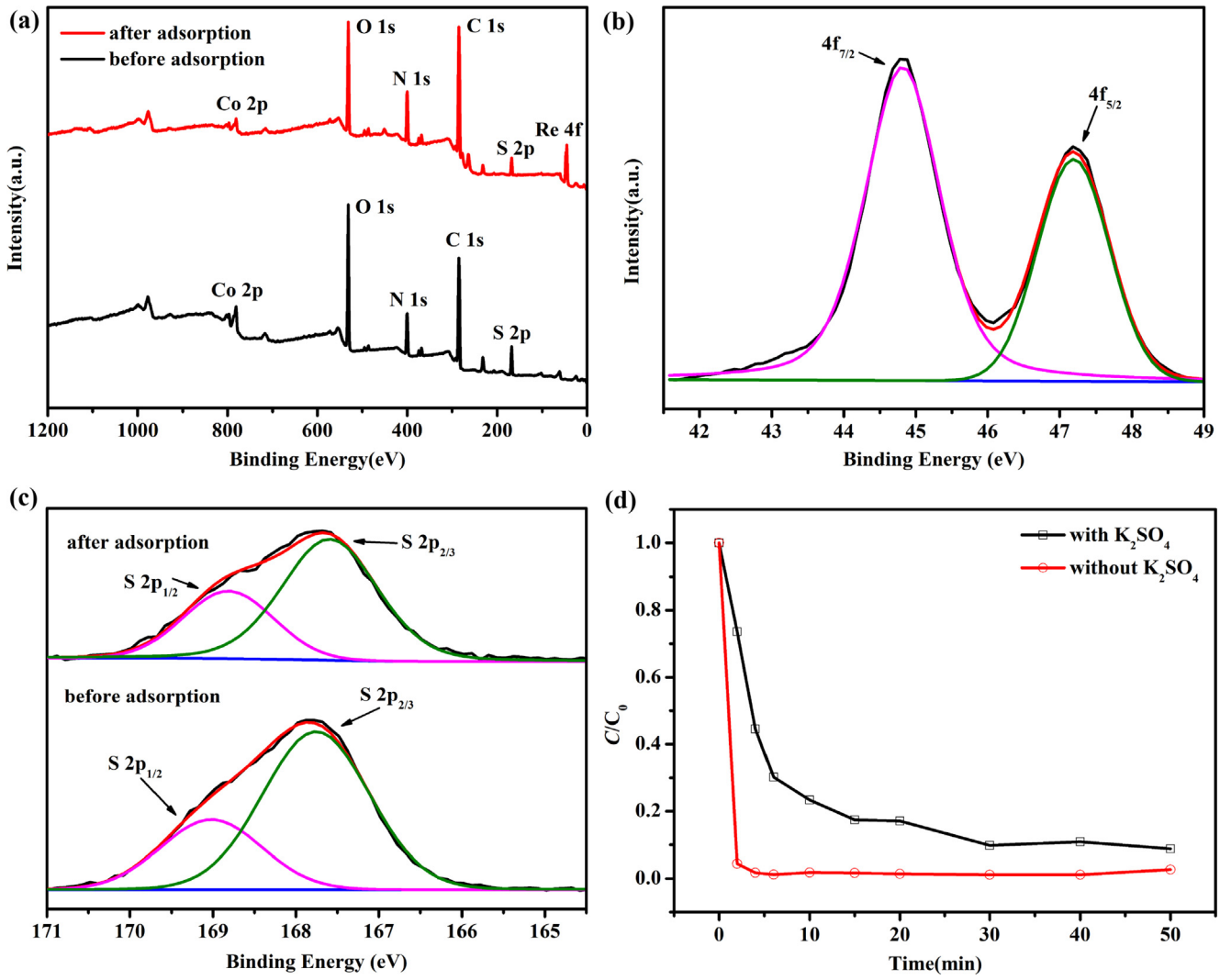

Fig. 9. XPS spectra of (a) wide scan; narrow scan of (b) Re 4f (c) S 2p region for ReO_4^-; (d) adsorption efficiency of **BUC-17** for ReO_4^- in pure aqueous and saturated K_2SO_4 solution.

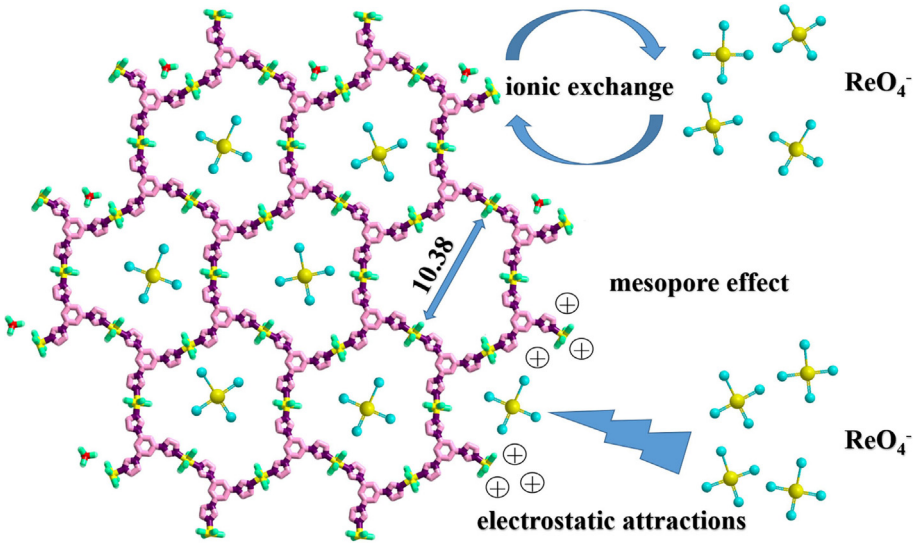

Fig. 10. Proposed reaction mechanism between ReO_4^- and **BUC-17.**

$4f_{7/2}$, which is blue-shifted in contrast with that of $KReO_4$ (46.1 eV) [75], verifying the electrostatic adsorption played an significant role in the adsorption of ReO_4^- by **BUC-17** [76]. The binding energy of 167.6 eV and 168.8 eV (S 2p) correspond to SO_4^{2-} decreased appreciably suggested the existence of ion-exchange interactions between ReO_4^- and **BUC-17** (Fig. 9c) [77]**.**Therefore, the possible sorption mechanism of **BUC-17** toward ReO_4^- can be clarified as both ion-exchange interactions and electrostatic interaction (Fig. 10).

4. Conclusion

In all, cationic MOF **BUC-17** with high water/alkaline stability was used to adsorb ReO_4^- and showed excellent adsorption capacity (401.9 mg g^{-1}), which was superior to most reported adsorbents. The adsorption of ReO_4^- onto **BUC-17** was fitted to the pseudo-second-order kinetic model and Langmuir isotherm. The adsorption process was spontaneous ($\Delta G^o < 0$), exothermic ($\Delta H^o < 0$) and the randomness increases ($\Delta S^o > 0$). Both electrostatic action and the uncoordinated anions SO_4^{2-} in **BUC-17** played an important role in adsorption, in where SO_4^{2-} would be easily exchanged by ReO_4^-. Besides, in a wide range of pH values (4.0–10.0) and high salinity, **BUC-17** could still adsorb ReO_4^- efficiently without decreased adsorption capacity. The SPE column experiments indicated that **BUC-17** could be the promising candidate for large-scale high concentration ReO_4^- removal from wastewater. This work provide insight to the adsorption behavior and mechanism of **BUC-17** toward ReO_4^-. Therefore, **BUC-17** was expected to accomplish adsorptive removal toward TcO_4^-.

Declaration of Competing Interest

The authors declare that they have no known competing financial interests or personal relationships that could have appeared to influence the work reported in this paper.

Acknowledgements

This work was supported by National Natural Science Foundation of China (51878023), Great Wall Scholars Training Program Project of Beijing Municipality Universities (CIT&TCD20180323), Beijing Talent Project (2020A27) and The Fundamental Research Funds for Beijing University of Civil Engineering and Architecture (X20147/X20141/X20135/X20146).

Appendix A. Supplementary data

Supplementary data to this article can be found online at https://doi.org/10.1016/j.poly.2021.115218.

References

[1] A.M. Omer, Renew. Sust. Energ. Rev. 12 (2008) 2265–2300.
[2] A. Goeppert, M. Czaun, J.P. Jones, G.K. Surya Prakash, G.A. Olah, Chem. Soc. Rev 43 (2014) 7995–8048.
[3] Y. Sun, Q. Wu, G.J.E. Shi, E. Science, Energy Environ. Sci. 4 (2011) 1113–1132.
[4] C.W. Abney, K.M. Taylor-Pashow, S.R. Russell, Y. Chen, R. Samantaray, J.V. Lockard, W. Lin, Chem. Mater. 26 (2014) 5231–5243.
[5] S. Ma, L. Huang, L. Ma, Y. Shim, S.M. Islam, P. Wang, L.-D. Zhao, S. Wang, G. Sun, X. Yang, J. Am. Chem. Soc. 137 (2015) 3670–3677.
[6] J. Shen, W. Chai, K. Wang, F. Zhang, ACS Appl. Mater. Interfaces 9 (2017) 22440–22448.
[7] H. Hu, L. Sun, Y. Gao, T. Wang, Y. Huang, C. Lv, Y.F. Zhang, Q. Huang, X. Chen, H. Wu, J. Hazard. Mater. 387 (2020) 121670.
[8] D. Banerjee, D. Kim, M.J. Schweiger, A.A. Kruger, P.K. Thallapally, Chem. Soc. Rev 45 (2016) 2724–2739.
[9] B. Gu, G.M. Brown, P.V. Bonnesen, L. Liang, B.A. Moyer, R. Ober, S.D. Alexandratos, Environ. Sci. Technol. 34 (2000) 1075–1080.
[10] S. Sarri, P. Misaelides, D. Zamboulis, X. Gaona, M. Altmaier, H. Geckeis, J. Radioanal. Nucl. Chem. 307 (2016) 681–689.
[11] E.A. Katayev, G.V. Kolesnikov, J.L. Sessler, Chem. Soc. Rev 38 (2009) 1572–1586.
[12] Q. Ding, F. Ding, T. Qian, D. Zhao, L. Wang, Water, Air, Soil Pollut. 226 (2015) 1–10.
[13] J. Li, C. Chen, R. Zhang, X. Wang, Sci. China Chem. 59 (2016) 150–158.
[14] L. Mei, F.Z. Li, J.H. Lan, C.Z. Wang, C. Xu, H. Deng, Q.Y. Wu, K.Q. Hu, L. Wang, Z.F. Chai, J. Chen, J.K. Gibson, W.Q. Shi, Nat. Commun. 10 (2019) 1–12.
[15] R.J. Drout, K. Otake, A.J. Howarth, T. Islamoglu, L. Zhu, C. Xiao, S. Wang, O.K. Farha, Chem. Mater. 30 (2018) 1277–1284.
[16] C. Xiao, M.A. Silver, S. Wang, Dalton Trans. 46 (2017) 16381–16386.
[17] C. Zhao, X. Pan, Z. Wang, C.-C. Wang, Chem. Eng. J. (2020), https://doi.org/10.1016/j.cej.2020.128022.
[18] Z. Hasan, S.H. Jhung, J. Hazard. Mater. 283 (2015) 329–339.
[19] C.-C. Wang, X.-H. Yi, P. Wang, Appl. Catal. B: Environ. 247 (2019) 24–48.
[20] C.-C. Wang, X.-D. Du, J. Li, X.-X. Guo, P. Wang, J. Zhang, Appl. Catal. B: Environ. 193 (2016) 198–216.
[21] C.-C. Wang, J.-R. Li, X.-L. Lv, Y.-Q. Zhang, G. Guo, Energy Environ. Sci. 7 (2014) 2831–2867.
[22] X.-Y. Xu, C. Chu, H. Fu, X.-D. Du, P. Wang, W. Zheng, C.-C. Wang, Chem. Eng. J. 350 (2018) 436–444.
[23] X.-H. Yi, S.-Q. Ma, X.-D. Du, C. Zhao, H. Fu, P. Wang, C.-C. Wang, Chem. Eng. J. 375 (2019), https://doi.org/121910.121016/j.cej.122019.121944 121944.
[24] H. Zhang, L. Dai, Y. Feng, Y. Xu, Y. Liu, G. Guo, H. Dai, C. Wang, C. Wang, H.-C. Hsi, H. Huang, J. Deng, Appl. Catal. B: Environ. 275 (2020), https://doi.org/119010.111016/j.apcatb.112020.119011 119011.
[25] J.-W. Wang, F.-G. Qiu, P. Wang, C. Ge, C.-C. Wang, J. Clean. Prod. 279 (2021), https://doi.org/123410.121016/j.jclepro.122020.123408 123408.
[26] C.-C. Wang, X. Wang, W. Liu, Chem. Eng. J. 391 (2020), https://doi.org/123610.121016/j.cej.122019.123601 123601.
[27] X.-D. Du, C.-C. Wang, J. Zhong, J.-G. Liu, Y.-X. Li, P. Wang, J. Environ. Chem. Eng. 5 (2017) 1866–1873.
[28] J.J. Li, C.C. Wang, H.F. Fu, J.R. Cui, P. Xu, J. Guo, J.R. Li, Dalton Trans. 46 (2017) 10197–10201.
[29] X.-X. Song, H. Fu, P. Wang, H.-Y. Li, Y.-Q. Zhang, C.-C. Wang, J. Colloid Interface Sci. 532 (2018) 598–604.
[30] A. Nuhnen, D. Dietrich, S. Millan, C. Janiak, A.C.S. Appl, Mater. Interfaces 10 (2018) 33589–33600.
[31] H. Fu, X. Wang, P. Wang, Z. Wang, H. Ren, C.C. Wang, Dalton Trans. 47 (2018) 9014–9020.
[32] M. Bagheri, M.Y. Masoomi, A. Morsali, A. Schoedel, A.C.S. Appl, Mater. Interfaces 8 (2016) 21472–21479.
[33] A. Liu, C.C. Wang, C.Z. Wang, H.F. Fu, W. Peng, Y.L. Cao, H.Y. Chu, A.F. Du, J. Colloid Interface Sci. 512 (2018) 730–739.
[34] Y.-X. Li, Y.-C. Han, C.-C. Wang, Chem. Eng. J. 405 (2021), https://doi.org/10.1016/j.cej.2020.126648.
[35] N. Shen, Z. Yang, S. Liu, X. Dai, C. Xiao, K. Taylor-Pashow, D. Li, C. Yang, J. Li, Y. Zhang, M. Zhang, R. Zhou, Z. Chai, S. Wang, Nat. Commun. 11 (2020) 1–12.
[36] X. Zhao, C. Mao, K.T. Luong, Q. Lin, Q.G. Zhai, P. Feng, X. Bu, Angew. Chem. Int. Ed. 55 (2016) 2768–2772.
[37] D. Banerjee, W. Xu, Z. Nie, L.E.V. Johnson, C. Coghlan, M.L. Sushko, D. Kim, M.J. Schweiger, A.A. Kruger, C.J. Doonan, P.K. Thallapally, Inorg. Chem. 55 (2016) 8241–8243.
[38] Y. Li, Z. Yang, Y. Wang, Z. Bai, T. Zheng, X. Dai, S. Liu, D. Gui, W. Liu, M. Chen, Nat. Commun. 8 (2017) 1–11.
[39] L. Zhu, D. Sheng, C. Xu, X. Dai, M.A. Silver, J. Li, P. Li, Y. Wang, Y. Wang, L. Chen, C. Xiao, J. Chen, R. Zhou, C. Zhang, O.K. Farha, Z. Chai, T.E. Albrecht-Schmitt, S. Wang, J. Am. Chem. Soc. 139 (2017) 14873–14876.
[40] D. Sheng, L. Zhu, X. Dai, C. Xu, P. Li, C.I. Pearce, C. Xiao, J. Chen, R. Zhou, T. Duan, O.K. Farha, Z. Chai, S. Wang, Angew. Chem. Int. Ed. 58 (2019) 4968–4972.
[41] N. Shen, Z. Yang, S. Liu, X. Dai, C. Xiao, K. Taylor-Pashow, D. Li, C. Yang, J. Li, Y. Zhang, Nat. Commun. 11 (2020) 1–12.
[42] D. Pang, P. Wang, H. Fu, C. Zhao, C.-C. Wang, S.N. Appl, Sci. 2 (2020) 1–11.
[43] J. Guo, J.-J. Li, C.-C. Wang, J. Environ. Chem. Eng. 7 (2019), https://doi.org/102910.101016/j.jece.102019.102909 102909.
[44] D. Li, J.C. Seaman, S.E.H. Murph, D.I. Kaplan, K. Taylor-Pashow, R. Feng, H. Chang, M. Tandukar, J. Hazard. Mater. 374 (2019) 177–185.
[45] C. Xu, S. Peng, C. Tan, H. Ang, H. Tan, H. Zhang, Q. Yan, J. Mate. Chem. A 2 (2014) 5597–5601.
[46] Y. Ho, J. Hazard. Mater. 136 (2006) 681–689.
[47] Q. Xu, Y. Wang, L. Jin, Y. Wang, M. Qin, J. Hazard. Mater. 339 (2017) 91–99.
[48] X. Guo, Z. Ma, D. Li, D. Yu, J. Mol. Liq. 297 (2020), https://doi.org/111910.111016/j.molliq.112019.111901 111901.
[49] Q. Liao, D. Zou, W. Pan, W. Linghu, R. Shen, Y. Jin, G. Feng, X. Li, F. Ye, A.M. Asiri, H.M. Marwani, Y. Zhu, X. Wu, W. Dong, J. Mol. Liq. 258 (2018) 275–284.
[50] T.W. Weber, R.K. Chakravorti, AIChE J. 20 (1974) 228–238.
[51] W.J. Weber, J.C. Morris, J. Sanit. Eng. Div. 90 (1964) 79–108.
[52] K.V. Kumar, K. Porkodi, J. Hazard. Mater. 146 (2007) 214–226.
[53] A.A. El-Zahhar, N.S. Awwad, E.E. El-Katori, J. Mol. Liq. 199 (2014) 454–461.
[54] D. Pang, C.-C. Wang, P. Wang, W. Liu, H. Fu, C. Zhao, Chemosphere 254 (2020), https://doi.org/126810.121016/j.chemosphere.122020.126829 126829.
[55] Y. Wang, H. Gao, J. Colloid Interface Sci. 301 (2006) 19–26.
[56] H. Fei, M.R. Bresler, S.R. Oliver, J. Am. Chem. Soc. 133 (2011) 11110–11113.
[57] S. Wang, E.V. Alekseev, J. Diwu, W.H. Casey, B.L. Phillips, W. Depmeier, T.E. Albrecht-Schmitt, Angew. Chem. Int. Ed. 49 (2010) 1057–1060.

[58] S. Wang, P. Yu, B.A. Purse, M.J. Orta, J. Diwu, W.H. Casey, B.L. Phillips, E.V. Alekseev, W. Depmeier, D.T. Hobbs, T.E. Albrecht-Schmitt, Adv. Funct. Mater. 22 (2012) 2241–2250.
[59] X. Shu, L. Shen, Y. Wei, D. Hua, J. Mol. Liq. 211 (2015) 621–627.
[60] Z. Lou, Z. Zhao, Y. Li, W. Shan, Y. Xiong, D. Fang, S. Yue, S. Zang, Bioresour. Technol. 133 (2013) 546–554.
[61] J. Li, C. Chen, R. Zhang, X. Wang, Sci. China Chem. 59 (2015) 150–158.
[62] C.-P. Li, J.-Y. Ai, H. Zhou, Q. Chen, Y. Yang, H. He, M. Du, Chem. Commun. 55 (2019) 1841–1844.
[63] Z. Wang, J. Zhang, Q. Wu, X. Han, M. Zhang, W. Liu, X. Yao, J. Feng, S. Dong, J. Sun, Chemosphere 248 (2020), https://doi.org/126010.121016/j.chemosphere.122020.126042 126042.
[64] A.R. Tehrani-Bagha, H. Nikkar, N.M. Mahmoodi, M. Markazi, F.M. Menger, Desalination 266 (2011) 274–280.
[65] D. Dechojarassri, S. Omote, K. Nishida, T. Omura, H. Yamaguchi, T. Furuike, H. Tamura, J. Hazard. Mater. 355 (2018) 154–161.
[66] S. Simsek, Z.M. Senol, H.I. Ulusoy, J. Hazard. Mater. 338 (2017) 437–446.
[67] A. Sari, M. Tuzen, J. Hazard. Mater. 164 (2009) 1372–1378.
[68] P. Karthikeyan, S. Meenakshi, J. Mol. Liq. 296 (2019), https://doi.org/111710.111016/j.molliq.112019.111766 111766.
[69] X.-D. Du, C.-C. Wang, J.-G. Liu, X.-D. Zhao, J. Zhong, Y.-X. Li, J. Li, P. Wang, J. Colloid Interface Sci. 506 (2017) 437–441.
[70] W. Wang, M. Li, Q. Zeng, Sep. Purif. Technol. 149 (2015) 16–23.
[71] Y. Peng, H. Huang, Y. Zhang, C. Kang, S. Chen, L. Song, D. Liu, C. Zhong, Nat. Commun. 9 (2018) 1–9.
[72] X.-X. Huang, L.-G. Qiu, W. Zhang, Y.-P. Yuan, X. Jiang, A.-J. Xie, Y.-H. Shen, J.-F. Zhu, CrystEngComm 14 (2012) 1613–1617.
[73] Y. Pan, Y. Pang, Y. Shi, W. Zheng, Y. Long, Y. Huang, H. Zheng, Microchim. Acta 186 (2019) 1–8.
[74] Z. Yan, Z. Xu, B. Cheng, C. Jiang, Appl. Surf. Sci. 404 (2017) 426–434.
[75] Q. Sun, L. Zhu, B. Aguila, P.K. Thallapally, C. Xu, J. Chen, S. Wang, D. Rogers, S. Ma, Nat. Commun. 10 (2019) 1–9.
[76] M. Ding, L. Chen, Y. Xu, B. Chen, J. Ding, R. Wu, C. Huang, Y. He, Y. Jin, C. Xia, Chem. Eng. J. 380 (2020), https://doi.org/122510.121016/j.cej.122019.122581 122581.
[77] W. Fu, H. Chen, S. Yang, W. Huang, Z. Huang, Chemosphere 232 (2019) 9–17.